TESTING AND EVALUATION OF THERMAL BARRIER COATINGS

Robert Vaßen[1], Yutaka Kagawa[2], Ramesh Subramanian[3], Paul Zombo[3], Dongming Zhu[4]

[1] Forschungszentrum Jülich GmbH, IEK-1, 52425 Jülich, Germany

[2] Research Center for Advanced Science and Technology, The University of Tokyo, Tokyo 153-8904, Japan

[3] Siemens Energy Inc., Orlando FL 32826, USA

[4] NASA Glenn Research Center at Lewis Field, Cleveland, OH 44135, USA

Abstract

Thermal barrier coatings are complex systems with properties largely depending on the specific microstructure. A further difficulty arises from the fact that properties change during operation time, typically leading to degradation. This degradation also depends on the specific loading conditions which can be rather complex. Different laboratory set-ups are described which are able to simulate, at least partially, the actual loading conditions. In addition, sensing and non-destructive methods are described which are targeted towards a reliable operation of a gas-turbine engine with thermal barrier coated components.

Introduction

Testing thermal barrier coating (TBC) systems and evaluating their performance in-service present major challenges. First and foremost, the conditions under which they operate are often extremely harsh, combining high temperatures, steep temperature gradients, fast temperature transients, high pressures, additional mechanical loading, as well as oxidative and corrosive environments. These are difficult to reproduce in the laboratory. The coating system also changes with time at temperature as inter-diffusion occurs, microstructures evolve and the properties of the constituent multilayer materials change. For instance, the oxide top-coat sinters, increasing both its thermal conductivity and elastic modulus, but the rate of sintering depends on its purity. Furthermore, the properties that need to be evaluated are rarely those of the constituent bulk materials themselves. For instance, while the intrinsic fracture toughness of the ceramic top-coat typically made 7 wt% yttria stabilized zirconia (7YSZ) is important, it is the toughness that a delamination crack experiences as it extends in or near the interface with the thermally grown oxide (TGO) that directly influences the lifetime under thermal cycling conditions. As coatings become prime-reliant, meaning that they can be implemented into the design of the engine with reliable performance criteria, it is also essential to develop sensors and non-destructive evaluation methods to monitor TBC temperatures, the extent of sub-critical delamination in service as well as identifying manufacturing flaws, while also creating an artificial intelligence supervisory system that can be implemented in the field to provide feedback to the manufacturing and design sectors for product improvement. Several sensor approaches are being explored, including infrared imaging, Raman spectroscopy, thermography, impedance spectroscopy, acoustic emission and luminescence sensing [1, 2, 3, 4, 5, 6].

Mechanical Properties

One of the fundamental problems in discussing and evaluating the mechanical properties of coatings is establishing the appropriate value is and at what microstructural scale it should be determined. This is especially so of the oxide top-coat since considerable variability and uncertainty arises from the porous nature of the coating as well as its anisotropy and microstructural evolution at elevated temperature. For simple properties, such as the overall thermal expansion mismatch stresses on thermal cycling and the available elastic strain energy release rate, the macroscopic biaxial Young's modulus, such as determined by a macroscopic mechanical test is generally adequate, recognizing that it can be expected to be different under tension than compression. By contrast, the local modulus obtained by nano-indentation pertains to the modulus of the intrinsic material and local stiffness but not to the generation of average thermal cycling induced stresses. The same issue pertains to distinguishing macroscopic and local thermal conductivity. For this reason, there is intensive interest in using local information, obtained from nanoindentation, for instance, together with tomographic images to predict overall properties using object-oriented finite element methods, like the OOF tool available on the NIST web page [7].

While this is a very promising methodology, it is less suited to understanding or predicting crack growth since these do not depend on only average mechanical properties. At small crack lengths, crack growth rates are mainly controlled by the intrinsic fracture toughness. For YSZ this is unusually high for an oxide and has recently been attributed to ferroelastic domain switching [8]. Understanding the toughening processes in YSZ also provides guidance for the selection and design of new TBC materials with enhanced toughness levels. One of the surprising results of recent measurements has been that fracture toughness for long cracks in TBCs, for instance those associated with coating delamination, is three to four times higher than the intrinsic toughness, as illustrated in Fig. 1. While it has always been recognized that microstructure must play a role in the fracture of TBCs the magnitude of the toughening enhancement, of the order of 150 N/m [9] and extent of the R-curve (rising toughness) is considerably larger than anticipated. The origin of the R-curve in plasma-sprayed and electron-beam physical vapor deposited (EB-PVD) TBCs is now known to differ in detail but is essentially due to local crack deflections resulting in a tortuous crack path forming microstructural heterogeneities whose relative motion during crack propagation results in friction. Details on crack path and toughening mechanisms are discussed in Refs. [9, 10].

Thermal Gradient Testing

Testing coatings under extreme temperature gradients and heat flux conditions approximating actual engine operation poses special challenges. One approach has been to use a high-power CO_2 laser rig [11], such as implemented at NASA Glenn Research Center, and the other is to use a flame rig configuration in which heat is applied on one side by an oxygen/hydrocarbon gas flame [12]. In both cases the samples are cooled from the back side with a high-pressure compressed air jet. While these configurations are not suitable for testing complex shaped blades and vanes, these new testing platforms can be used to evaluate rates of sintering, thermal cycle lifetimes, thermal conductivities, and monitor damage evolution under high-flux conditions of planar TBC systems, such as coated superalloy buttons. These configurations also allow for the introduction of particulates (sand, ash), water and salt during testing, as shown in Fig. 2 [13] to evaluate the degradation they may cause. At high surface temperature, or with particulates addition, this type of testing typically results in a subsequent chipping of surface layers due to the thermal gradient present (see article by Levi *et al.*). Actual coating failure modes identified from engine testing or from service operation are usually complex, largely depending on excursions from standard engine operating conditions, and processed coating composition, architecture and microstructures. Nevertheless, once a particular failure mode has been identified, the tests can be used to evaluate coatings under similar conditions.

Since the initial development of the steady-state CO_2 laser (wavelength 10.6 μm) test facility at NASA and its application to measuring the sintering of coatings and thermal conductivity, for instance [14, 15, 16], its capabilities have subsequently been extended. Amongst the most recent is evaluating interface crack propagation under extreme heat flux, cyclic loading conditions [17] such as might occur during repeated aircraft take-off. Figure 3 shows the test results of a 127 μm thick, precracked TBC specimen. The initial ceramic surface temperature was set at approximately 1287°C and 20-min heating/cooling cycles and 60 to 100 W/cm^2 heat flux. The coating surface temperature increased continuously as the crack propagates, whereas the metal backside temperature remained relatively constant. The apparent coating thermal conductivity, calculated from the known laser heat flux, decreases as the delamination crack grew until the test was interrupted by spallation of the coating after about 200 cycles. The crack propagation process has also been monitored independently by a high sensitivity video camera, for calibrating the crack propagation with cycles. From these data, the crack propagation rate (*da/dN)* and the laser thermal transient stress associated stress intensity factor amplitude (ΔK) for a plasma sprayed 7-8YSZ were also determined [17]. The results show slower thermal fatigue crack propagation rates compared to monolithic ceramics indicative of additional R-curve toughening effects due to the roughness and plasticity at or near the ceramic/metal interface.

Thermomechanical Fatigue

As with other high-temperature materials, including superalloys, thermomechanical fatigue (TMF) can adversely influence coating durability [18, 19, 20, 21]. The origin of TMF is creep and plastic deformation in each of the component layers in the TBC system driven by coefficient of thermal expansion (CTE) mismatch, especially the CTE mismatch between the bond-coat, the superalloy and the top-coat under thermal gradient conditions, as well as mechanical loads, such as centrifugal force. Testing under TMF conditions is essential but the wide variety of possible in-phase mechanical and temperature loadings and out-of-phase loadings conditions as well as realistic thermal gradient conditions makes this a demanding materials engineering task that is only now being addressed. Even so there have been surprises. One is that contrary to initial expectation, compressive deformation is the major form of damage in strain-controlled in-phase and stress-controlled out-of-phase modes [22]. Another is that cracks can nucleate in the bond-coat at high-temperatures and propagate into the superalloy. Figure 4 illustrates several of the loading configurations and characteristic damage accumulation behavior in EB-PVD TBC systems under in-phase stress-controlled TMF test mode [23, 24]. Stress/strain-time, and numbers of loading cycles, under in-phase TMF test conditions are consistent with the creep behavior of superalloys, as reported elsewhere (Fig. 4a). Ratcheting behavior superimposes on the creep behavior as illustrated in Fig. 4b. This behavior is consistent with most of the applied load being supported by the superalloy. However, the creep behavior of the EB-PVD TBC layer is interesting: at 1150 °C the layer can deform up to about 8% tensile strain without evidence of visible cracking [25]. With increasing tensile creep strain, cracking of the TBC layer initiates, and ultimately, multiple fragmentation behavior occurs, as seen in Figs. 4c and 4d. It is found that the cracks in the TBC layer do not propagate through the entire thickness and the spacing (Fig. 4d) is much smaller than that predicted using continuum mechanics [26]. In addition, TMF tests on samples with a center-hole clearly demonstrate that cracking is related to tensile stress/strain concentrations [24]. Following cracking of the TBC layer, void formation in the bond coat below the cracks can occur and new oxide forms in the exposed alloy. The width of the cracks in the TBC layer typically has a wide distribution and the cracks below the cracked TBC layer propagate to different depths (Fig.s 4c and 4f). The evidence suggests that there is a sequence of cracking in the TBC oxide. After cracking of the TBC, the life is similar to that of the bare superalloy. Another form of damage is the large area delamination where the bond-coat and superalloy are locally exposed to higher temperatures (Fig. 4g).

Sensing and Non-Destructive Evaluation (NDE)

Concurrent with developments in testing the mechanical properties of TBC systems, there have been explorations of new sensing approaches. For instance, as the temperatures at the TBC surface and at the TGO are critical parameters, there has been an emphasis on non-contact methods of measuring temperature at these locations. One method that shows particular promise is luminescence sensing based on the dependence of photoluminescence lifetime on temperature [27, 28, 29, 30]. It deals with using luminescence to monitor delamination. In this method, luminescent rare-earth ions are incorporated into the crystal structure of the YSZ coating during deposition of the coating so that they are localized, for instance, at the ceramic top-coat/TGO interface and then again at the top-coat surface. Then, at temperature their luminescence is stimulated by a pulsed laser and the excited luminescence collected and its luminescence decay monitored. In addition to being a non-contact method, the rare-earth dopant can also be localized to a smaller depth than the optical penetration depth in optical pyrometry giving superior depth resolution. This temperature sensing methodology has recently been demonstrated using an EB-PVD 7YSZ TBCs [27, 30, 31]. The experiment setup is illustrated in Fig. 5A. A solid-state frequency doubled YAG:Nd laser emitting at 532 nm illuminates the center of the coating surface, while the main high heat flux CO_2 laser was used for heating the specimens under large thermal gradients. A sapphire light pipe was positioned to collect the excited luminescence signal during the testing. Figure 5B shows the luminescence sensor measured real-time interface temperature under various heat flux conditions, demonstrating the ability to collect luminescence from a thin embedded sensor layer in a thermal barrier coating systems under high temperature thermal gradients.

Key to the extending the use of TBCs is assessing damage, especially sub-critical coating delamination, prior to coating failure. In particular, early detection of TBC damage also enables a part to be replaced and, possibly, repaired. The majority of non-destructive methods for this type of monitoring utilize spectral variations in the optical properties of YSZ. For instance, at 10.6 μm, the wavelength of CO_2 lasers, YSZ is heavily absorbing but it is translucent in the visible and near infrared (IR), so one approach is to image local separations between the coating and alloy based on variations in reflectivity of thermal waves launched by pulse heating of the coating surface. The larger effusivity at the delamination than at the interface between the TBC and the underlying alloy locally causes a greater thermal reflectivity and hence higher image contrast enabling an image to be formed of large delaminations. In the visible, YSZ is transparent but highly scattering. However, in the mid-IR, the scattering is reduced, enabling optical imaging of delaminations in both EB-PVD and plasma-sprayed TBCs [31].

Recently, it has also been demonstrated that with advances in IR focal plane array cameras, it is now possible to perform real-time, on-line near-IR monitoring of rotating blades during engine operation. This offers the prospect of increasing gas turbine operational reliability, especially by minimizing engine shut-down or outage time. In addition, with a link to component computer aided design (CAD) models, thermal design models can be validated by *in situ* temperature measurements. This is expected to enable a better diagnosis and prognostics of component integrity for more advanced engine operation. As the technology of focal plane imaging has become more sophisticated, the number, types and pixels of array detectors has greatly increased, and, together with more selective filtering capabilities, these detectors can more efficiently be matched to specific applications, improving measurement performance. When used with complex algorithms to provide real time linearization and compensation of the detector output, higher precision temperature measurements become feasible. For instance, to measure the temperatures of high speed rotating components using focal plane technology, requires very short integration (< 3 ms) or the ability to have photons fill the focal plane to form a snap shot in micro seconds and even nano seconds, thus creating qualitative spatial detail of the rotating blade. In effect, every imaging pixel is a pyrometer. In a recent Siemens implementation, a telescopic lens system is used to image a portion of the blades onto a focal plane array over the spectral range of 0.9 μm to 1.6 μm, avoiding characteristic emissions from combustion from gas species, such as CO_2 and H_2O, while also maximizing the sensitivity of the array to the peak of the black body radiation from the blades.

Radiation reaching the detector includes contributions from three sources: 1) radiation emitted from the surface of the turbine component being imaged, 2) reflected radiation included from particulates in the gas stream as well as, 3) radiation emitted from hot gases and particles in the field of view. A methodology was developed to overcome these hurdles and finally perform the surface temperature measurements. Figure 6 illustrates features that can be seen during the engine operation using state–of-the-art focal plane arrays with advanced software imaging. These include (a) TBC spallation on the leading edge of the blade as seen by dark edge of TBC, (b) local heating due to platform rub – bright feature near rub, (c) local cooling at platform – dark due to cooling air leakage (d) Platform TBC delamination, observed as bright/dark line corresponding to a buckled TBC, (e) overlapping cooling holes, with the dark cooling streams are not giving good coverage and (f) Platform TBC crack observed as a faint bright line, verified by visual picture shown in the inset in Fig. 6.

One exciting development in inspection methods is combing thermal imaging with ultrasonics. The concept is to energize a component or an array of blades, for instance, with an ultrasonic source and use a highly sensitive focal plane array to image the locations of frictional heating. This has recently been implemented, for instance, in the Siemens acoustic thermography, SIEMAT® for the detection of cracks and kissing bonds in parts. Its attributes include a high sensitivity to tight interfaces, the ability to see defects through coatings, and the ability to inspect components with minimal preparation [33, 24, 35]. Post processing algorithms are then used to assist in the identification of defects.

Summary and Outlook

It is abundantly clear that testing and evaluation of TBCs is extremely challenging, yet TBCs progress depends critically on our ability to test, evaluate, and monitor TBCs under conditions relevant to engine operation. New methods for measuring mechanical properties of TBCs will need to be developed with a deep understanding of TBCs failure mechanisms. TMF and thermal gradient testing under realistic engine conditions are also needed to simulate more accurately TBC failure that is represenative of what happens in operating engines. Sensing, NDE, and *in situ* monitoring of TBC health are critical for the intelligent operation of engines with maximum utilization of TBCs and to avoid catastrophic failure.

Figure Captions

1. Crack resistance of inter-splat cracks and R-curve from extension of long delamination cracks in WOL (wedge opening loading).

2. Photograph of the Julich gas burner rig heating a disk-shaped TBC sample with back-side compressed air cooling. In the central part of the flame a solution of CMAS is injected to spray it onto the hot-surface.

3. Laser heat flux thermal gradient cyclic test results of a 127 μm thick, precracked TBC specimen subject to 20 min heating and 4 min cooling thermal cycling. The initial circular crack was 2 mm in diameter. The effective thermal conductivity clearly correlates with the crack propagation until the coating spalled after 200 cycles.

4. Examples of typical behavior and damages in a EB-PVD TBC system during in-phase TMF testing mode: (a) creep curve, (b) ratcheting behavior, (c) TBC layer cracking (polished section, parallel to loading axis), (d) multiple fragmentation of TBC layer, (e) void formation in BC layer, (f) fatigue crack growth and new TGO formation in BC layer, (g) delamination of TBC layer, (h) illustration of anisotropic TGO morphology (arrow, loading direction), (i) example of stress distribution in TGO layer.

5. (a) Experimental setup for measuring the thermal barrier coating/metal interface temperature through the TBC by luminescence under laser high heat flux thermal gradient tests [27]. (b) TBC interface temperature measured as function of TBC surface and metal back surface temperatures with various heat fluxes, for two EB-PVD coating thicknesses. A good correlation of the sensor measurements with the heat flux measurements have been observed with the embedded Eu-YSZ sensor at high temperature [27, 31].

6. Example of possible features observed by an IR camera, during engine operation, at 3600 rpm with gas path temperatures higher than 1200 ˚C. Pictures are “still” frames of rotating blades.

References

[1] F. Yu, T. D. Bennett, *J Appl. Phys.*, **98**, 103501 (2005).

[2] K.W. Schlichting, K. Vaidyanathan, Y.H. Sohn, E.H. Jordan, M. Gell, N.P. Padture, *Mater. Sci. Engr.*, **A291**, 68 (2000).

[3] A.L. Heyes, J. P. Feist, X. Chen, Z. Mutasim, J. R. Nicholls, *J Engr. Gas Turbines and Power*, **130**, 061301 (2008).

[4] S. Song, P. Xiao, Mater. Sci. Engr., **B97**, 46 (2003).

[5] D. Renusch, M. Schütze, Surf. Coat. Technol., **202,** 740 (2007).

[6] P.G. Bison, S. Marinetti, E. Grinzato, V.P. Vavilov, F. Cernuschi, D. Robba, *Proc. SPIE*, **5073**, 318 (2003).

[7] http://www.nist.gov/mml/ctcms/oof/index.cfm

[8] C. Mercer, J.R. Williams, D.R. Clarke, A.G. Evans, *Proc. Roy. Soc.*, **A463**, 1393 (2007).

[9] J. Malzbender, T. Wakui, E. Wessel, R.W. Steinbrech, *Fract. Mech. Ceram.*, **14,** 435 (2005).

[10] M. Dononue, N.R. Philips, M.R. Begley, C.G. Levi, *Acta Mater.*, in press (2012).

[11] D. Zhu, R. A. Miller, *J. Mater. Res*., **14**, 146 (1999).

[12] F. Traeger, R. Vaßen, K.-H. Rauwald, D. Stöver, *Adv. Engr. Mater*., **5**, 429 (2003).

[13] T. Steinke, D. Sebold, D.E. Mack, R. Vaßen, D. Stöver, *Surf. Coat. Technol*., **205**, 2287 (2010).

[14] D. Zhu, R. A. Miller, *J. Therm. Spray Technol*., **9**, 175 (2000).

[15] D. Zhu, R. A. Miller, B. A. Nagaraj, R. W. Bruce, *Surf. Coat. Technol*., **138,** 1 (2001).

[16] D. Zhu, R. A. Miller, *MRS Bull.*, **27**, 43 (2000).

[17] D. Zhu, S. R. Choi, R. A. Miller, *Surf. Coat. Technol*., **188-189**, 146 (2004).

[18] B. Baufeld, E. Tzimas, H. Mullejans, S. Peteves, J. Bressers, W. Stamm, *Mater. Sci. Engr.,* **A315**, 231 (2001).

[19] A. Peichl, T. Beck, O. Vohringer, *Surf. Coat. Technol.*, **162,** 113 (2003).

[20] E. Tzimas, H. Mullejans, S.D. Peteves, J. Bressers, W. Stamm, *Acta Mater*., **48**, 4699 (2000).

[21] P.K. Wright, *Mater. Sci. Engr*., **A245**, 191 (1998).

[22] R. Kitazawa and Y. Kagawa, in preparation (2012).

[23] R. Kitazawa, M. Tanaka, Y. Kagawa, Y.F. Liu, *Mater. Sci. Engr*., **B 173**, 130 (2010).

[24] M. Tanaka, C. Mercer, Y. Kagawa, A.G. Evans, *J. Am. Ceram. Soc.,* **94**, 128 (2011).

[25] R. Kitazawa, H. Kakisawa, Y. Kagawa, *Surf. Coat. Technol.*, to be submitted (2012).

[26] M. Tanaka, Y.F. Liu, S.S. Kim, Y. Kagawa, *J. Mater. Res.*, **23**, 2382 (2008).

[27] M. M. Gentleman, J. I. Eldridge, D. M. Zhu, K.S. Murphy, D.R. Clarke, *Surf. Coat. Technol.*, **201,** 3937 (2006).

[28] M. D. Chambers, D. R. Clarke, *Ann. Rev. Mater. Res.*, **39**, 325 (2009).

[29] A. Rabhiou, J. Feist, A. Kempf, S. Skinner, A. Heyes, *Sensors and Actuators*, **A 169**, 18 (2011).

[30] J. I. Eldridge and D. Zhu, D. E. Wolfe, *Ceram. Eng. Sci. Proc.*, **32**, 3 (2011).

[31] M. M. Gentleman, Ph.D. Thesis, University of California, Santa Barbara (2007).

[32] J. I. Eldridge, C. M. Spuckler, R. E. Martin, *Intl. J. Appl. Ceram. Technol.,* **3,** 94 (2006).

[33] C. Homma, M. Rothenfusser, J. Baumann, R. Shannon, *Proc. Rev. Prog. Quant. NDE, AIP*, 566 (2006).

[34] X. Han, V. Loggins, Z. Zeng, L.D. Favro, R.L. Thomas, Appl. Phys. Lett., 1332 (2004).

[35] M. Rothenfusser, and C. Homma, , *Proc. Rev. Prog. Quant. NDE, AIP*, 624 (2005).

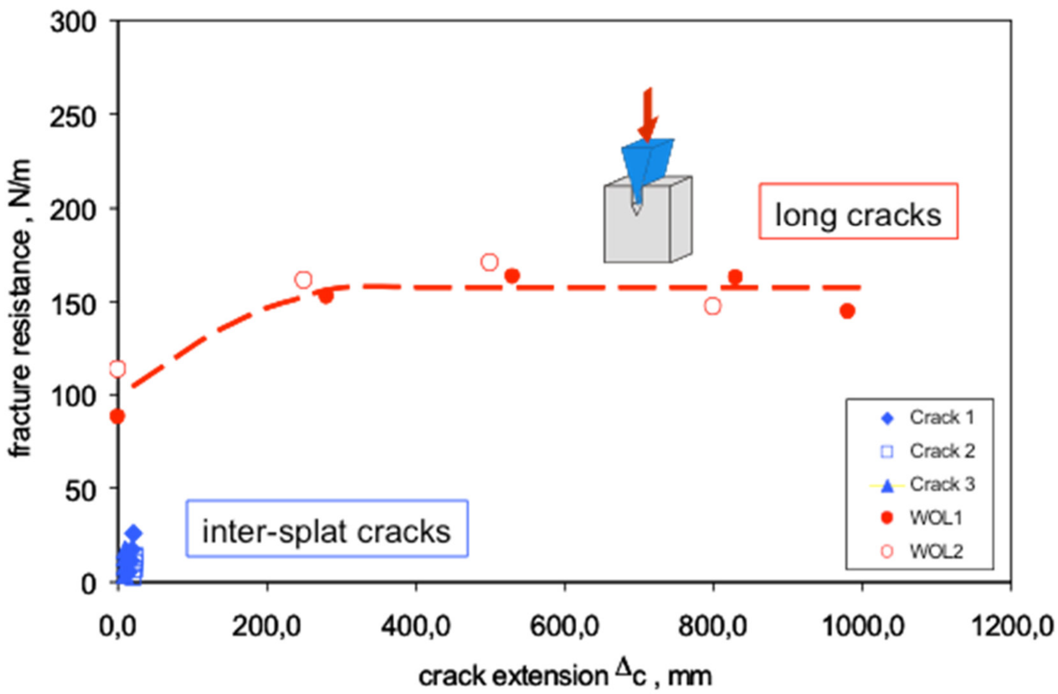
300
250
200
150
100
50
0
fracture resistance , N/m
0,0
200,0
400,0
600,0
800,0
1000,0
1200,0
crack extension Δc , mm
long cracks
inter-splat cracks
Crack 1
Crack 2
Crack 3
WOL1
WOL2

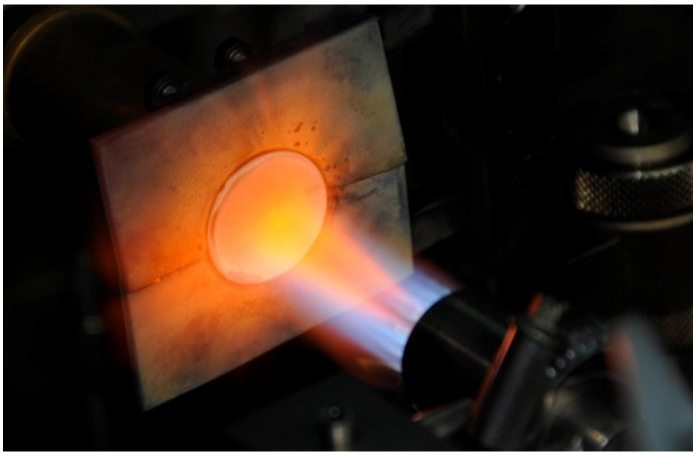

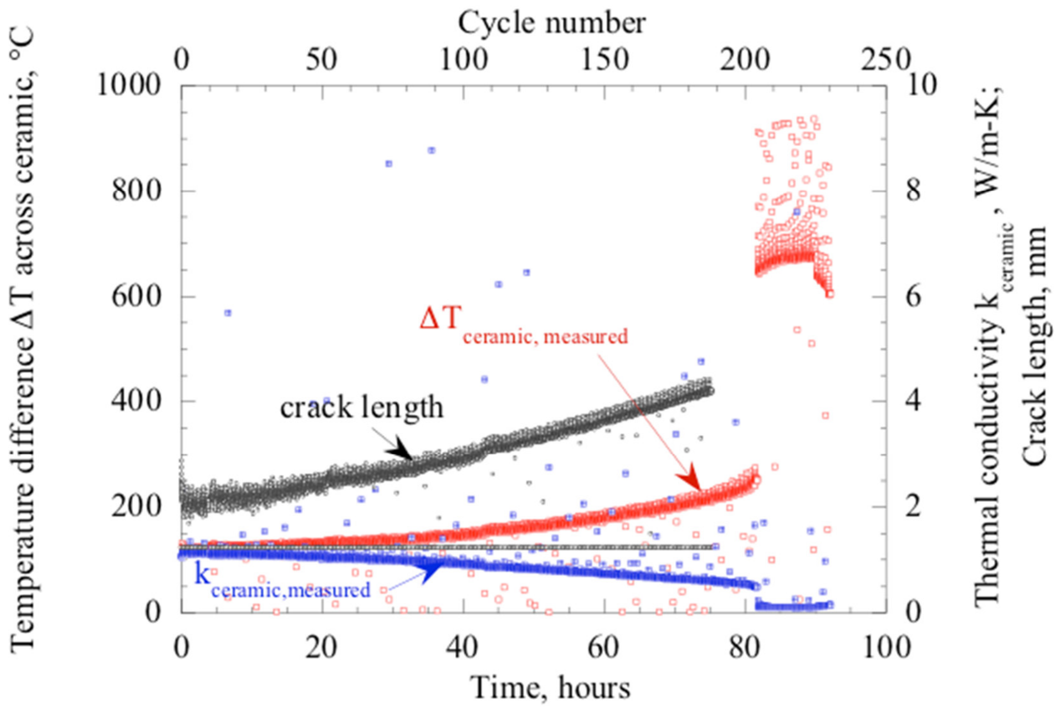

Cycle number
0
50
100
150
200
250
Temperature difference ΔT across ceramic, °C
1000
800
600
400
200
0
Thermal conductivity k ceramic, W/m-K; Crack length, mm
10
8
6
4
2
0
ΔT ceramic, measured
crack length
k ceramic,measured
0
20
40
60
80
100
Time, hours

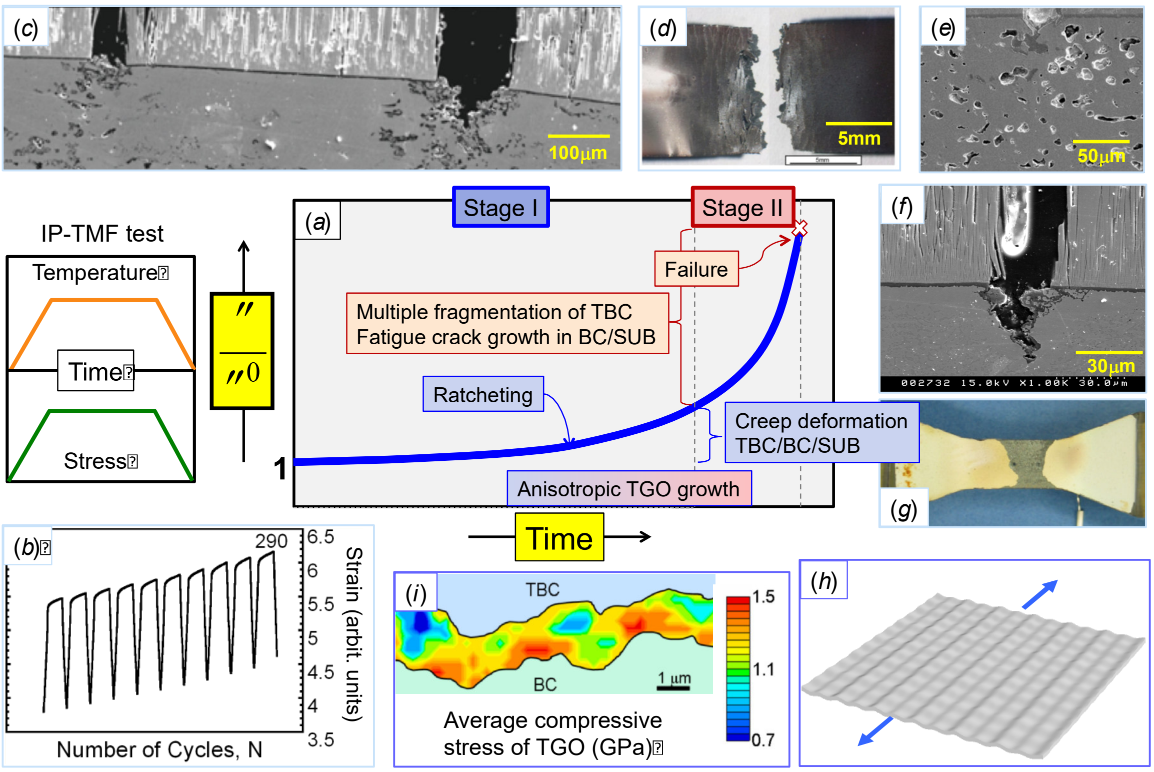

(c)
100μm
(d)
5mm
(e)
50μm
IP-TMF test
Temperature
Time
Stress
(a)
Stage I
Stage II
Failure
Multiple fragmentation of TBC
Fatigue crack growth in BC/SUB
Ratcheting
Creep deformation
TBC/BC/SUB
Anisotropic TGO growth
1
Time
(f)
30μm
(g)
(b)
290
Number of Cycles, N
6.5
6
5.5
5
4.5
4
3.5
Strain (arbit. units)
(i)
TBC
BC
1 μm
1.5
1.1
0.7
Average compressive
stress of TGO (GPa)
(h)

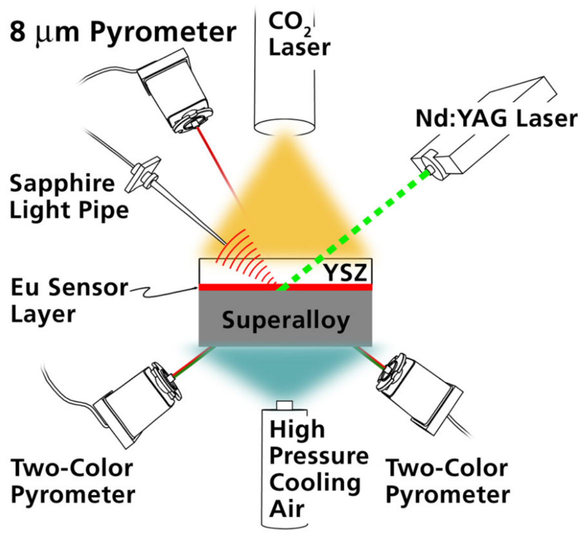
8 μm Pyrometer
CO2 Laser
Nd:YAG Laser
Sapphire Light Pipe
Eu Sensor Layer
YSZ
Superalloy
Two-Color Pyrometer
High Pressure Cooling Air
Two-Color Pyrometer

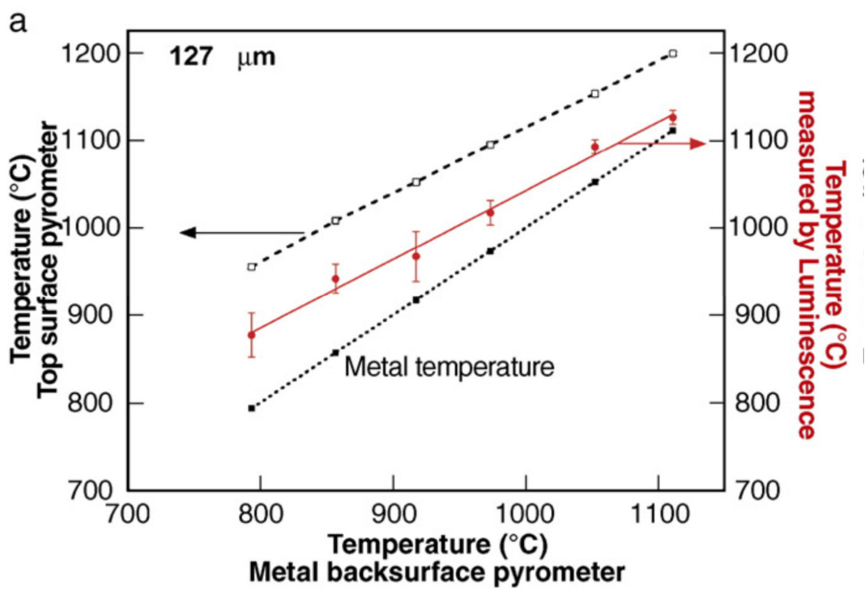
a
127 μm
Temperature (°C) Top surface pyrometer
Temperature (°C) measured by Luminescence
Metal temperature
Temperature (°C) Metal backsurface pyrometer
700
800
900
1000
1100
1200

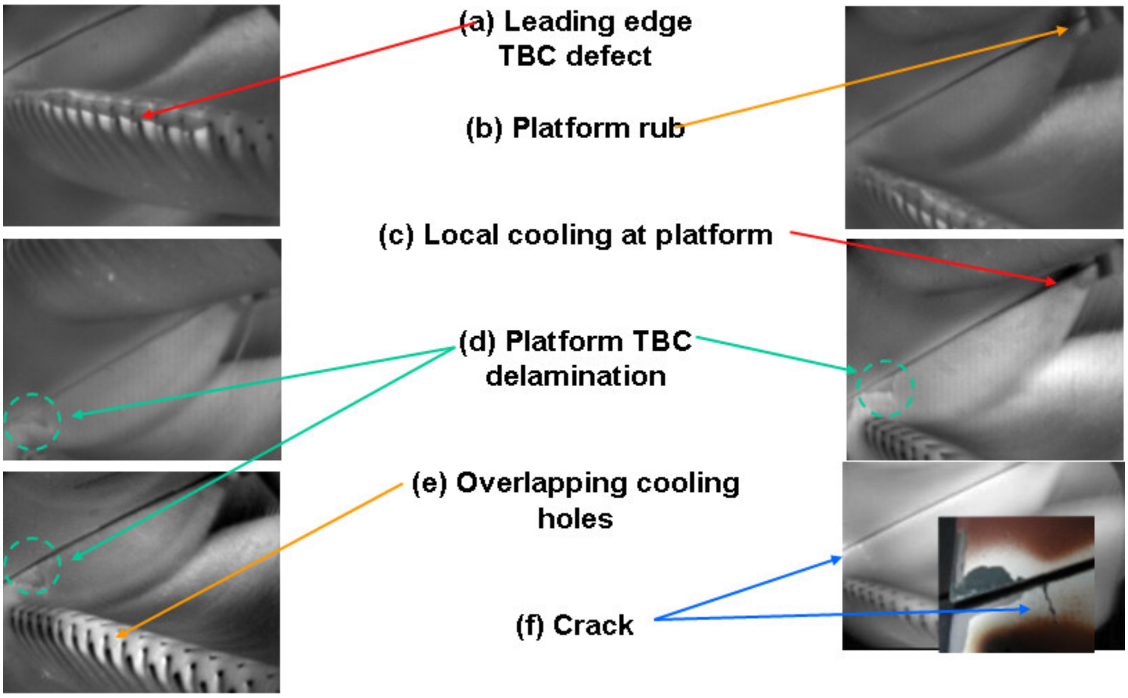
(a) Leading edge
TBC defect
(b) Platform rub
(c) Local cooling at platform
(d) Platform TBC
delamination
(e) Overlapping cooling
holes
(f) Crack